Publication I

Juha T. Toivanen, Tommi A. Laitinen, and Pertti Vainikainen. Modified test zone field compensation for small-antenna measurements. IEEE Transactions on Antennas and Propagation, accepted for publication.

Modified Test Zone Field Compensation for Small-Antenna Measurements

Juha T. Toivanen, Tommi A. Laitinen, Pertti Vainikainen

***Abstract*—A method is presented by which full 3-D antenna pattern measurements can be performed without an anechoic measurement environment. The method is a field compensation technique that allows compensating for the effect of arbitrary incident test zone fields. Simulations are performed to demonstrate that the method works reliably in various kinds of surroundings. The applicability range of the method is estimated in terms of the accuracy of the determined far-field antenna pattern with a given uncertainty in individual measurement values. Finally, measurement results are presented that are in line with the simulations and verify the functioning of the method.**

***Index Terms*—Antenna measurement, error correction, field compensation, radiation pattern, test zone.**

I. Introduction

THE past decades have seen a considerable amount of research on compensation and correction methods for antenna range imperfections. These methods are applied in order to improve the measurement accuracy by reducing the effect of the non-ideal measurement environment on the measurement result. Often, despite the use of anechoic chambers, the reflections from the measurement surroundings constitute an important error source, which can be further minimized through the use of numerical correction techniques.

Examples of such techniques are the deconvolution [1], plane-wave synthesis [2], antenna pattern correction [3] [4], virtual array [5], test zone field (TZF) compensation [6], plane wave, pattern subtraction method [7], EAD method [8], MARS technique [9], and IsoFilter technique. Typical limitations in these techniques are the increased measurement time or equipment requirements, limited field models, or restrictions on the level or number of the reflection components.

One promising correction method is the TZF compensation technique [6]. In this technique, a complete spherical-wave model is created for the test zone fields, using a minimum amount of extra equipment and measurements. The traditional first-order probe correction technique is then iteratively employed to correct for not only the higher-order azimuthal spherical modes of the probe pattern but also for the undesired reflections present in the measurement chamber. The technique is computationally efficient and thus applicable for electrically large antennas. However, the drawback of this technique is that constraints are placed on the amplitude of the reflected signals relative to the direct signal. The application of the technique may thus not be possible in environments with a high reflectivity level.

The purpose of this paper is to present a general field compensation method, which, as opposed to [6], can be applied in practically any kind of (stable) electromagnetic environment. This way, one gains the advantage of not needing expensive anechoic measurement facilities. The method is a variation of the technique presented in [6]. It is theoretically exact, assuming negligible multiple reflections between the antenna under test (AUT) and the surroundings; it accounts for all range reflections and interfering signals of constant nature.

The idea of this method was briefly introduced in [11]. The method is presented in this paper in a more comprehensive manner, including the theoretical background, computer simulations, and measurements. Application to both single- and multi-probe ranges is discussed in detail. Additionally, an uncertainty analysis is presented that provides information on the applicability of the method under different measurement noise levels.

The results of this paper are important in that they present a way to perform antenna pattern measurements without any RF-absorber coating in the measurement facility. The presented method is best suited for measurement of small antennas (e.g., with the radius of the minimum sphere of 2-5 λ at maximum), where the computational requirements remain reasonable. It can be applied in both near-field and far-field conditions.

II. Compensation Method

The modified test zone field compensation method is presented for the case where the range probe acts as the transmitter and the antenna placed in the test zone as the receiver. It is, however, applicable also for the opposite case. The method comprises two steps. In the first step (Sec. II.A), the TZF is determined by measuring a calibration antenna (with known radiation characteristics) in the test zone. In the second step (Sec. II.B), the knowledge of the TZF is utilized

Manuscript received April 9, 2009. This work has been funded by the Academy of Finland. Financial support has also been provided by Nordforsk, by The Finnish Foundation for Economic and Technology Sciences, by HPY Research Foundation, by The Finnish Society of Electronics Engineers, by Walter Ahlström's Foundation, and by Ella and Georg Ehrnrooth's Foundation.

J. T. Toivanen, T. A. Laitinen, and P. Vainikainen are with the Aalto University School of Science and Technology, Department of Radio Science and Engineering, SMARAD, P.O. Box 13000, FI-00076 Aalto, Finland, phone: 358-9-4512252, fax: 358-9-4512152, e-mail: juha.toivanen@tkk.fi.

in solving the radiation characteristics of the AUT.

It is first assumed that there is only one single-polarized range probe. The generalization to dual- or multi-polarized probes and multi-probe measurement systems is discussed in Sec. II.C.

A. Test Zone Field Measurement

The compensation method is based on the spherical-wave theory and the TZF and the antenna radiation characteristics are expressed in this context. The first task is to determine the TZF produced by the range probe, with respect to a fixed TZF coordinate system. For this, a calibration antenna, known as the TZF probe, is required. The TZF probe must be larger than the AUTs to be measured, so that it is sensitive to a large-enough number of spherical modes. Alternatively, a small TZF probe can be used provided that it is offset from the test zone origin so that its minimum measurement sphere is larger than the AUT minimum sphere. The radiation characteristics of the TZF probe must be known from a separate calibration measurement. They are expressed by the antenna transmission coefficients T_{smn}, which relate to the spherical wave expansion of the field radiated by an antenna as

$$\overline{E}(r,\theta,\varphi) = \frac{k}{\sqrt{\eta}} \sum_{smn} v\, T_{smn} \overline{F}^{(3)}_{smn}(r,\theta,\varphi). \tag{1}$$

Here, $\overline{E}(r,\theta,\varphi)$ is the electric field strength in a position given by the spherical coordinates r, θ, and φ; k is the wave number; η is the wave admittance; v is the input signal; and $\overline{F}^{(3)}_{smn}(r,\theta,\varphi)$ are the outgoing spherical vector wave functions. It is well known, how to determine the T_{smn} from spherical antenna measurements [12], and hence it is not discussed here.

The TZF probe is measured in different orientations in the test zone. It is necessary to express the T_{smn} of the TZF probe in the fixed TZF coordinate system. Therefore, the transmission coefficients depend on the probe's orientation in the TZF coordinate system, denoted by the Euler angles φ, θ, and χ. The conversion of T_{smn} to the TZF coordinate system is accomplished with the spherical-wave rotation function $d^{n}_{m\mu}$ [12].

$$T_{s\mu n}(\varphi,\theta,\chi) = \sum_{m} T_{smn} e^{-im\chi} d^{n}_{\mu m}(-\theta) e^{-i\mu\varphi}. \tag{2}$$

In the formula above, the change in notation (T_{smn} => $T_{s\mu n}$) signifies the change of coordinate system. Next, the $T_{s\mu n}$ are converted to receiving coefficients $R_{s\mu n}$ through the simple relation

$$R_{s\mu n}(\varphi,\theta,\chi) = (-1)^{\mu} T_{s,-\mu,n}(\varphi,\theta,\chi). \tag{3}$$

So, now there is a separate set of receiving coefficients $R_{s\mu n}$ for each orientation of the TZF probe, all expressed in the same TZF coordinate system.

Using the spherical-wave theory, the signal received by an antenna placed in a test zone can be expressed as [12]

$$w = \sum_{s\mu n} R_{s\mu n} Q^{(4)}_{s\mu n}. \tag{4}$$

In this formula, w is the received signal, $R_{s\mu n}$ are the receiving coefficients of the antenna, and $Q^{(4)}_{s\mu n}$ are the spherical-wave-expansion coefficients of the TZF. The superscript index 4 means that the coefficients represent the incoming waves. It will be dropped in the following for simplicity of notation. The spherical-mode index triplet (s,μ,n) can be converted into the single-index j-notation

$$j = 2\{n(n+1) + \mu - 1\} + s, \tag{5}$$

where the integer indices get the values s = {1, 2}, n = {1…N}, μ = {-n…n} and j = {1…J}. N is the so-called truncation number for the spherical-mode series and J is the total number of modes, with $J = 2N(N+2)$. Empirical formulas connect the required N with the size of the antenna [13] [14]. N is proportional to kr_0, where r_0 is the radius of the minimum sphere enclosing the antenna (in the TZF measurement, r_0 is also the radius of the test zone).

One can now use (2), (3), and (4) to form a system of linear equations for the $Q_{s\mu n}$. With the single-index notation (5), this system of linear equations is expressed in matrix form as

$$\begin{bmatrix} R_1(\varphi_1,\theta_1,\chi_1) & .. & R_J(\varphi_1,\theta_1,\chi_1) \\ R_1(\varphi_2,\theta_2,\chi_2) & .. & R_J(\varphi_2,\theta_2,\chi_2) \\ : & : & : \\ R_1(\varphi_M,\theta_M,\chi_M) & .. & R_J(\varphi_M,\theta_M,\chi_M) \end{bmatrix} \begin{bmatrix} Q_1 \\ : \\ Q_J \end{bmatrix} = \begin{bmatrix} w_1 \\ : \\ : \\ w_M \end{bmatrix}$$

or, in short,

$$\mathbf{Rq} = \mathbf{w}. \tag{6}$$

Here $\mathbf{R}$ is an M-by-J matrix such that each row corresponds to a different measurement orientation and M is the total number of orientations; J is the number of spherical modes, determined by the size of the TZF probe; $\mathbf{q}$ is a column vector containing the spherical-wave coefficients $Q_{s\mu n}$ of the TZF; and $\mathbf{w}$ is a column vector containing the measured signal values. Generally, $M \geq J$ is required so that there are at least as much linearly independent rows in the matrix as there are unknown variables. This matrix equation can be solved for the $Q_{s\mu n}$ using the Moore-Penrose pseudoinverse [15]

$$\mathbf{q} = \mathbf{R}^{\dagger}\mathbf{w} = \left(\mathbf{R}^{\mathrm{H}}\mathbf{R}\right)^{-1}\mathbf{R}^{\mathrm{H}}\mathbf{w}. \tag{7}$$

The $Q_{s\mu n}$ then contain all relevant information on the TZF, including the range probe signal, the reflected and scattered

signals, and other interfering signals. They provide a complete characterization of the fields entering the test zone.

B. AUT Measurement

In the AUT measurement, the $Q_{s\mu n}$ are used to solve the AUT radiation pattern through a similar procedure that was used in the TZF measurement. In this part, the TZF coordinate system is no longer used. Instead, the $Q_{s\mu n}$ are converted to the AUT coordinate system. With the AUT orientation in the TZF coordinate system denoted by φ, θ, and χ, the $Q_{s\mu n}$ in the AUT coordinate system are given as

$$Q_{smn}(\varphi,\theta,\chi)=\sum_{\mu} Q_{s\mu n} e^{i\mu\varphi} d^{n}_{m\mu}(\theta) e^{im\chi}. \tag{8}$$

Now, by placing the AUT in the test zone and measuring the signal w for different AUT orientations (different values for φ, θ, χ), one can use (4) and (8) to form a system of linear equations for the R_{smn} coefficients of the AUT. Again, using the single-index notation (5), one obtains the matrix equation

$$\begin{bmatrix} Q_1(\varphi_1,\theta_1,\chi_1) & .. & Q_J(\varphi_1,\theta_1,\chi_1) \\ Q_1(\varphi_2,\theta_2,\chi_2) & .. & Q_J(\varphi_2,\theta_2,\chi_2) \\ : & : & : \\ Q_1(\varphi_M,\theta_M,\chi_M) & .. & Q_J(\varphi_M,\theta_M,\chi_M) \end{bmatrix} \begin{bmatrix} R_1 \\ : \\ R_J \end{bmatrix} = \begin{bmatrix} w_1 \\ : \\ : \\ w_M \end{bmatrix}$$

or,

$$\mathbf{Qr} = \mathbf{w}. \tag{9}$$

Q is an M-by-J matrix such that each row corresponds to a different measurement orientation and M is the total number of orientations; J is the required number of spherical modes, determined by the size of the AUT; **r** is a column vector containing the receiving coefficients R_{smn} of the AUT and **w** is a column vector containing the measured signal values. Again, $M \geq J$ is required but here both M and J may be smaller than in the TZF measurement, if the AUT is smaller than the TZF probe. The solution is obtained through the pseudoinverse

$$\mathbf{r} = \mathbf{Q}^{\dagger}\mathbf{w} = \left(\mathbf{Q}^{\mathrm{H}}\mathbf{Q}\right)^{-1}\mathbf{Q}^{\mathrm{H}}\mathbf{w}. \tag{10}$$

This gives the measurement result since, combining (1) and (3), the radiation pattern of the AUT can be calculated from

$$\overline{E}(r,\theta,\varphi)=\frac{k}{\sqrt{\eta}}\sum_{smn} v\,(-1)^m R_{s,-m,n}\,\overline{F}^{(3)}_{smn}(r,\theta,\varphi). \tag{11}$$

The pseudoinverse gives the least-squares solution to the problem through a single matrix multiplication since $\mathbf{Q}^{\dagger}$ can be calculated in advance and applied for all AUTs that fit within the test zone. The measurement point locations can be chosen at will, bearing in mind that the more diversity they exhibit (in terms of polarization and direction) the less sensitive to measurement noise the result will be.

C. Multi-Probe Measurement Systems

The modified TZF compensation method can be applied also with multi-polarized range probes and multi-probe antenna measurement systems. In this case, the TZF is different for each probe and therefore, the TZF coefficients become a function of the probe (P).

$$Q_{s\mu n} \rightarrow Q_{s\mu n}(P) \tag{12}$$

Thus, the TZF measurement and calculations must be repeated for all range probes. In practice, the signals corresponding to every range probe can be recorded in one scan with the TZF probe, provided that the measurement setup does not involve movement or rotation of the range probes during the measurement.

Intuitively, one needs less measurement orientations for the AUT, when using a multi-probe system, compared to a single-probe system. This is also the case with the presented method. When it is applied for a multi-probe range, the number of rows in the **Q** matrix in (9) is multiplied by the number of probes, because, as discussed above, each probe produces a different TZF. The **Q** matrix then gets the form

$$\mathbf{Q} = \begin{bmatrix} Q_1(\varphi_1,\theta_1,\chi_1,P_1) & .. & Q_J(\varphi_1,\theta_1,\chi_1,P_1) \\ : & .. & : \\ Q_1(\varphi_M,\theta_M,\chi_M,P_1) & .. & Q_J(\varphi_M,\theta_M,\chi_M,P_1) \\ : & .. & : \\ Q_1(\varphi_1,\theta_1,\chi_1,P_K) & .. & Q_J(\varphi_1,\theta_1,\chi_1,P_K) \\ : & .. & : \\ Q_1(\varphi_M,\theta_M,\chi_M,P_K) & .. & Q_J(\varphi_M,\theta_M,\chi_M,P_K) \end{bmatrix} \tag{13}$$

where P_k denotes probe number k and there are in total K probes. Similarly, the measurement-value vector **w** will contain values measured with every range probe.

$$\mathbf{w} = \left[w_1(P_1)\,..\,w_M(P_1)\ \ldots\ w_1(P_K)\,..\,w_M(P_K)\right]^{\mathrm{T}}. \tag{14}$$

Naturally, in this case the number of AUT measurement orientations can be reduced, while still obtaining enough linearly independent rows to be able to solve the matrix equation. In the extreme case, a large number of measurement probes are placed all around the AUT so that no AUT rotation at all is required. In this case,

$$\mathbf{Q} = \begin{bmatrix} Q_1(P_1) & .. & Q_J(P_1) \\ Q_1(P_2) & .. & Q_J(P_2) \\ : & .. & : \\ Q_1(P_K) & .. & Q_J(P_K) \end{bmatrix} \quad (15)$$

and

$$\mathbf{w} = \left[w(P_1) \;\; w(P_2) \;\; ... \;\; w(P_K) \right]^{\mathrm{T}}. \quad (16)$$

In fact, this is the case with the measurements presented later in this paper in Sec. V.

An added benefit is that in a multi-probe system, the TZF compensation provides also the channel balance calibration (as shown in [11]) since the information about the channel-response differences is included in the TZFs.

III. Simulations

A virtual antenna measurement environment is created in MatLAB, which allows the testing of the compensation method in a large number of different environments through simulations. The simulations are performed in a virtual measurement range with a single, dual-polarized range probe.

A. Simulation Environment

The simulation consists of a range probe, TZF probe, AUT, and several reflectors, which are modeled by short dipoles. The number, location, amplitude and polarization of the reflectors are varied. The AUT is a mobile terminal antenna model with a maximum directivity of 4.7 dBi [16]. A dual-ridged horn antenna model (directivity 9.5 dBi) is used as the range probe and also as the TZF probe. The number of reflections in the simulations is between 1 and 10 and the amplitude varies between −20 dB and 0 dB compared to the range probe signal in the test zone. The simulation proceeds through the following steps:

1. Definition of the radiation characteristics of all antennas
2. Definition of the reflector locations and signals
3. Calculation of the true TZF
4. Virtual measurement of the TZF using the TZF probe
5. Addition of noise to the measurement values
6. Calculation of the TZF from the noisy measurement values
7. Virtual measurement of the AUT
8. Addition of noise to the measurement values
9. Application of the compensation using the TZF calculated from the noisy measurement values
10. Calculation of the measured AUT radiation pattern and comparison with the true pattern

The measurement noise, which is added to all measurement values, has a Gaussian distribution. The number of spherical modes used for the AUT is $J = 48$. An oversampling factor of approximately 2 is used in all virtual antenna measurements, meaning the number of measurement points is approximately twice the number of modes.

B. Simulation Results

The results of this analysis are presented in terms of the uncertainty in the total radiated power (TRP) and the directivity of the AUT, as derived from the antenna measurements. For each simulation run, the error in the directivity (ΔD), referenced to the true antenna pattern, is calculated for the full 4π space angle. The error values are normalized to the maximum directivity, i.e.,

$$\Delta D(\theta,\phi) = \frac{D_{meas}(\theta,\phi) - D_{true}(\theta,\phi)}{\max(D_{true})} \quad (17)$$

The root-mean-square (RMS) value of these directivity errors provides an average figure of merit for the accuracy of an antenna pattern measurement.

When the measurement noise is non-existent, the directivity and TRP errors are zero, meaning the method is theoretically exact. Of course, a realistic measurement scenario will include a certain level of noise and other sources of uncertainty. Fig. 1 shows the RMS directivity errors as a function of the maximum reflection amplitude (dBs relative to the direct range probe signal in the test zone), for different numbers of reflectors and different measurement noise levels. The graphs show a sliding average i.e., the RMS error values of all simulations within a 5-dB window are averaged to give a point on the graph. For readability, graphs are shown only for cases with 1 and 10 reflectors.

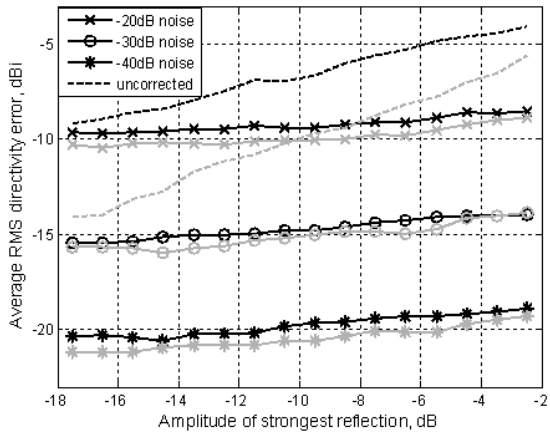

Fig. 1. Antenna pattern measurement accuracy for different noise levels (gray = 1 reflection, black = 10 reflections).

The number or amplitude of the reflections does not have a large influence on the overall uncertainty. The slight tilt of the graphs originates from the matrix inversion; the condition number of the **Q** matrix increases slightly (on average) with reflector amplitude and amount, resulting in higher uncertainty. Only the measurement noise level has a large

impact on the results. This overall noise level can be thought of as representing a number of different sources of uncertainty, such as positioning errors, multiple reflections, measurement instrument noise etc. It can be seen from Fig. 1 that Gaussian noise with −40 dB standard deviation (relative to the maximum received signal) causes on average an RMS directivity error of −20 dB and a 10-dB rise in the noise level causes a 5-dB rise in the directivity error. Even with −20 dB noise level, the pattern measurement accuracy can still be sufficient for, e.g., mobile terminal antenna measurements, where the highest accuracy is typically not required.

In Table I, the mean errors (in dBs) of the TRP values are shown for each noise level. The values are for the case with 10 reflectors and are shown as a function of the maximum reflection amplitude (*A*). It can be seen that without correction the error rises steadily with the reflection amplitude, as expected. The correction eliminates most of the error in all cases, regardless of the noise level. However, the higher the noise level, the more residual error still remains after the correction.

TABLE I
MEAN ERROR IN TOTAL RADIATED POWER [DB] (C = CORRECTED, U = UNCORRECTED).

Max refl. amplitude [dB]	Noise level [dB]					
	−20		−30		−40	
	C	U	C	U	C	U
−5<A<0	0.5	3.9	0.2	4.6	0.0	3.7
−10<A<−5	0.4	2.1	0.2	2.0	0.0	2.1
−15<A<−10	0.4	1.2	0.1	1.1	0.0	1.4
−20<A<−15	0.6	0.8	0.1	0.5	0.0	0.7

IV. EXPERIMENTAL VALIDATION – SINGLE-PROBE SYSTEM

The presented method is verified experimentally by measurements with a single-probe measurement system installed in a standard laboratory room without anechoic properties. This kind of a measurement environment produces reflected fields with high amplitude and thus enables proper testing of the presented compensation method.

A. Test Zone Field Measurement

The room, in which the measurements were performed, contained many metal objects and reflecting surfaces relatively close to the test zone. A single, dual-polarized range probe was installed in the room in approximately 3-m distance from the test zone. For both polarizations of the range probe, all signals entering the test zone were characterized with the TZF measurement. The TZF measurement set-up is shown in Fig. 2, where the TZF probe can be seen in the middle installed on a rotating arm, which enabled a full 360-degree azimuth scan (φ). Elevation scan (θ) and the change of measurement polarization (χ) were made possible by the probe holder design, which incorporated rotary joints for this purpose. A wideband, Vivaldi-type printed-circuit-board antenna element was used both as the range probe and as the TZF probe. The circular absorber sheet seen in Fig. 2 was used in order to reduce the back-lobe radiation of the TZF probe.

Fig. 2. Test zone field measurement with a calibration antenna.

The required number of measurement points in the TZF measurement is determined by the number of significant spherical modes of the TZF probe pattern, which is proportional to the square of the radius of the minimum measurement sphere of the probe. The mode series must be truncated appropriately. If the selected truncation number is too low, one runs into aliasing problems and if it is too high, the computational burden of the problem increases unnecessarily. That being said, the result is not extremely sensitive to the selection of the truncation number.

The T_{smn} of the TZF probe must be known from a separate measurement so its radiation characteristics were measured at the DTU-ESA Spherical Near-Field Antenna Test Facility, in the Technical University of Denmark [17]. Fig. 3 shows the spherical-mode spectrum of the TZF probe at 1.8 GHz. The spherical mode number in the horizontal axis corresponds to the *j*-notation (5). It can be seen from Fig. 3 that there exist relatively high modes up to about j = 150. After this, the modes attenuate rapidly. A truncation number of N = 8 was used throughout the measurement frequency range of 1-3 GHz, giving J = 160 modes.

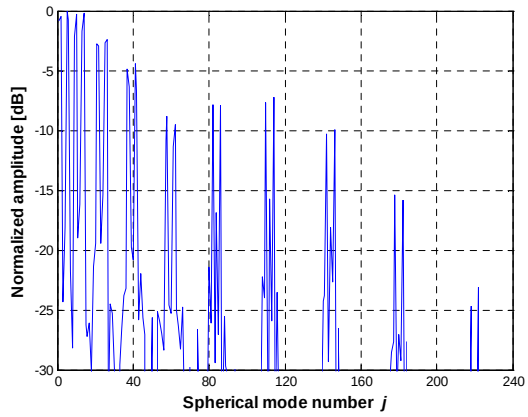

Fig. 3. The normalized transmission coefficients T_{smn} of the TZF probe at 1.8 GHz.

The number of measurement points should be somewhat higher than the number of modes. In the TZF measurement, a 20-degree step was chosen for both θ and φ and the measurement was performed in two polarizations, giving 292 measurement points in total. Therefore, with J = 160, the oversampling factor was approximately 1.8.

B. AUT Measurement

The test antenna (AUT1), a wideband horn antenna, is shown in Fig. 4. Its dimensions are 240 mm × 140 mm × 200 mm. Since AUT1 is similar in size to the TZF probe, a truncation number of N = 8 was used also in the AUT measurement. Also, the number of measurement points in the AUT measurement was the same as in the TZF measurement, with a 20-degree grid in both θ and φ. The measurement was performed in the range of 1-3 GHz with 100-MHz spacing.

Fig. 4. Measurement of AUT1 in a laboratory room with no RF-absorber coating on the walls.

C. Measurement Results

Based on the measurement data, the TZF compensation was applied as presented in Section II. The directivity of the AUT was calculated as a function of direction and compared with that provided by a reference measurement, which was performed at the DTU-ESA facility. A pattern cut at 2 GHz showing this comparison is presented in Fig. 5. Also the pattern measured without TZF compensation is shown and, as can be seen, it is severely distorted due to the high reflectivity level of the measurement room. The performance of the TZF compensation is good down to about −15 dB from the pattern maximum. Below this level, the measurement errors start to have a large effect and the compensation accuracy degrades.

The RMS directivity errors, calculated according to (17) assuming D_{true} to be equal to the DTU-ESA measurement value, are presented in Fig. 6. Without TZF compensation, the errors are in the range of −4 to −10 dB. Error levels this high can be expected, since the level of the strongest signal reflections in the measurement room was −5 to −10 dB compared to the direct range probe signal, depending on the frequency. Obviously the room is a very poor environment for antenna measurements.

Fig. 5 and Fig. 6 show that the application of the TZF compensation improves the results considerably. The average directivity error level after compensation is approximately −15 dB. There is no significant frequency dependence except that compensation accuracy is slightly limited at the lower end of the frequency range by the back-lobe radiation of the TZF probe.

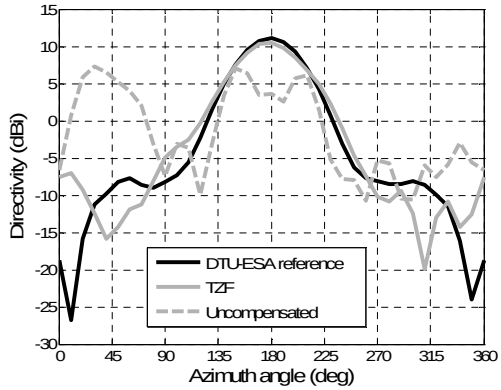

Fig. 5. Directivity of AUT1 with and without TZF compensation compared to the reference pattern.

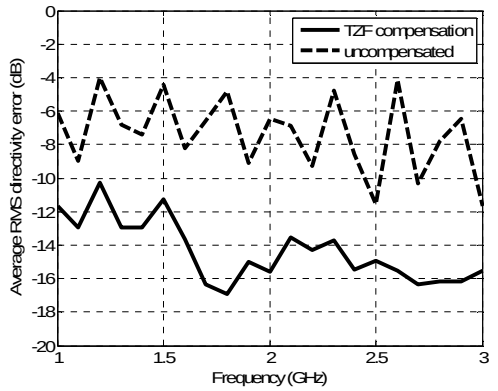

Fig. 6. Average directivity error as a function of the frequency with and without the TZF compensation.

D. Uncertainty Analysis

To estimate the measurement uncertainty in the TZF measurement, a control measurement was performed at regular intervals in a predetermined TZF probe position. The standard deviation of these values was approximately −40 dB relative to the maximum signal. This uncertainty is very low and, based on the simulation results in Sec. III.B, is not the limiting factor in the compensation accuracy.

There were more significant error sources in the measurements such as the rotating antenna support structure, which interferes with the TZF (and AUT) measurement since it is not stationary. Also, due to the back-lobe radiation of the TZF probe, the mounting flanges in the DTU-ESA calibration measurement and the actual TZF measurement affected the

pattern of the TZF probe in a different manner. Especially this was a problem at lower frequencies, where the level of the back-lobe radiation of the probe was higher. It is likely that these errors can be mitigated with better TZF probe and antenna holder designs.

V. Experimental Validation – Multi-Probe System

Tests of the presented method were also performed by measurements with a multi-probe range at the Department of Radio Science and Engineering in the Aalto University School of Science and Technology. This multi-probe range presents a suitable environment for the testing of the method, because the probes effectively act as a source of reflections in the measurement.

A. Test Zone Field Measurement

The measurements were performed with the multi-probe system presented in [18] and [19]. This system consists of 32 dual-polarized probes that are placed uniformly on a spherical surface. Uniform placement means here that the probe locations are those of the vertices of the concentric icosahedron and dodecahedron. The test zone is located in the centre of the sphere. The TZF probe, measurement grid, and other parameters are the same that were used in the single-probe measurements.

For every orientation of the TZF probe, a full measurement was performed, with each range probe at a time measuring the signal transmitted by the TZF probe (due to reciprocity, this is the same as considering the measurement probes as transmitters and the TZF probe as the receiver). This way, enough data was gathered for the characterization of the TZF corresponding to every measurement probe. The total amount of data is quite large, but the obtained data is valid as long as there are no significant changes in the system or in the measurement environment, and it can be used for all AUTs that fit within the characterized test zone. The scanning of the TZF probe was performed manually.

B. AUT Measurement

Three AUTs were used in the measurements. AUT2 is a simple sleeve dipole antenna, operating at 1.8 GHz. AUT3 and AUT4 are the two ports (left- and right-side elements, respectively) of the mobile terminal diversity antenna structure shown in Fig. 7. The model of AUT3 was used in the simulations in Sec. III. The dimensions of the whole antenna structure are 43 mm × 107 mm × 9 mm and it operates at 1.6 GHz.

All AUTs are relatively small in wavelengths. This means their spherical-mode spectrum does not extend very far and the used TZF probe is certainly large enough in comparison so that the required modes can be resolved. Due to the small size of the AUTs and the relatively small number of measurement probes, a truncation number of $N = 3$ was used in the measurements. The AUTs were measured by placing them in the centre of the test zone and recording the signal received by each measurement probe. The AUTs were measured in a single orientation. Due to the three-dimensional measurement probe configuration, sufficient measurement data was obtained without AUT rotation.

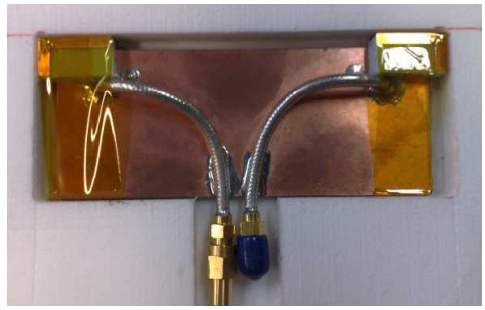

Fig. 7. Diversity antenna structure as AUT.

C. Measurement Results

Again, the TZF compensation was applied and the results calculated. Since the AUTs were not rotated during the measurements, the matrix **Q** and vector **w** in (9) were of the form in (15) and (16), respectively. The directivity values of the AUT were calculated as a function of direction and compared to the DTU-ESA reference measurement. The RMS directivity errors, calculated according to (17) assuming D_{true} to be equal to the DTU-ESA measurement value, are presented in Table II. The values are in the range of −7 to −10 dB for all AUTs. The error in TRP was also calculated and it was less than 0.4 dB for all AUTs.

Fig. 8 shows the E plane and H plane pattern cuts for the sleeve dipole (AUT2). In the H plane, the maximum difference between the DTU-ESA reference measurement and the measurement with the TZF compensation is approximately 0.7 dB. These differences are mainly caused by the errors in the TZF measurement (see uncertainty analysis in the next section). In the E plane, the pattern measured with the TZF compensation is smoother than the reference pattern. This is because the truncation number (and the number of measurement points) in the multi-probe measurement was smaller than in the DTU-ESA reference measurement. Thus, some of the pattern variation is averaged out in the multi-probe measurement.

A representative pattern cut for AUT3 is shown in Fig. 9, with a similar comparison between the multi-probe measurement and the DTU-ESA reference measurement. The accuracy of this measurement is of the same order as with AUT2, although on average the result is slightly better, as can be seen from Table II.

TABLE II
Normalized Directivity Errors for Measurements with the Modified TZF Compensation

AUT	Frequency [GHz]	RMS Directivity Error [dB]
AUT2	1.8	-7.4
AUT3	1.6	-9.7
AUT4	1.6	-8.1

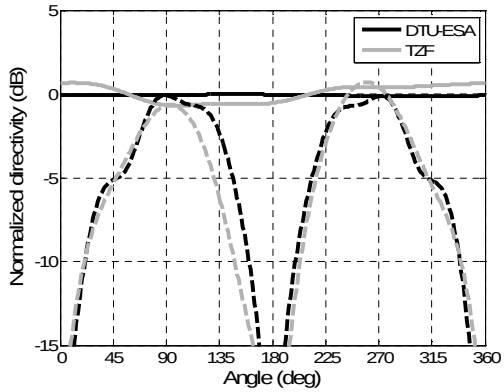

Fig. 8. E plane (dashed) and H plane (solid) pattern cuts for AUT2 (sleeve dipole). The multi-probe measurement with the TZF compensation is compared to the DTU-ESA reference measurement.

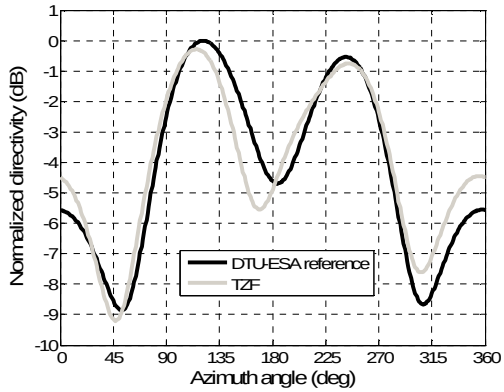

Fig. 9. AUT3 pattern cut, showing the DTU-ESA reference measurement and the multi-probe measurement with the TZF compensation.

D. Uncertainty Analysis

As in the single-probe measurements, a control measurement was performed at regular intervals in a predetermined TZF probe position to estimate the measurement uncertainty in the TZF measurement. The standard deviation of these values was approximately −25 dB relative to the maximum signal. This uncertainty is considerably higher than in the single-probe measurements and is mainly due to positioning errors because of the manual scanning. In addition, there are other error sources as mentioned in Sec. IV.D. The effect of the support structure of the TZF probe is now different since it is not present during the AUT measurement (AUT rotation was not required in the measurements).

Consequently, it seems realistic to assume that, when comparing the measurements with the simulation results, the overall measurement uncertainty in the measurements was comparable to the −20 dB noise level in the simulations. The reflectivity level in the measurement chamber has been earlier determined to be in the order of −20 dB. The reflections mostly originate from the probe antennas. With these parameters, the simulation results in Fig. 1 and Table I are in fairly good agreement with the measurement results.

VI. Discussion

It is worth attention to discuss the differences of the modified TZF compensation presented in this paper, as compared with the original TZF compensation presented in [6]. The essential difference between the two methods is the employed calculation technique. The modified TZF compensation uses a matrix-inverse solution method instead of the more traditional Fourier-transform-based method used in the original TZF compensation.

Several advantages are gained with the use of the matrix-inverse solution method. First, the solution is obtained directly; no iterations are required. Second, there are no limitations on the amplitude of the range reflections. Since the original TZF compensation is an iterative technique, the level of the range reflections must be lower than the range probe field for the iterative process to converge, whereas the modified TZF compensation, as presented here, can be used in a measurement chamber without any anechoic properties, i.e., without RF absorbers. Although for the measurements presented in this paper, the reflected fields were smaller in amplitude than the range probe field, in theory there are no restrictions in the method on the level of the reflected signals relative to the probe signal, because the probe signal has no special status in the method. As usual, however, the method does not compensate for multiple reflections between the AUT and the probes. Third, it is not necessary to use a measurement point grid that is regular in θ and φ. Instead, the measurement point locations can be chosen, e.g., to provide a uniform distribution over a spherical surface with no point clustering near the poles. This was also the case with the multi-probe measurements presented in this paper.

Actually, it is necessary to use the matrix inversion only in the second step of the modified TZF compensation, i.e., the AUT measurement, to realize the benefits discussed above. The TZF coefficients can be found in another way, e.g., as presented in [20], by using a so-called $\mu = \pm 1$ (first-order) probe as the TZF probe. However, the matrix-inverse solution method can be used also in the first step for the probe correction. This general probe correction method, although not often used, is known [21] and provides one additional advantage, namely the possibility to use a general (non-first-order) probe as the TZF probe. This makes it easier to find a suitable, wideband TZF probe for characterization of the TZF over a wide frequency band. In this paper, the matrix-inverse solution method is used in both the TZF measurement and the AUT measurement.

The downside of this solution method is that it is computationally demanding and potentially more sensitive to errors in the measurement data due to the matrix-inverse operation. The number of required spherical modes depends

on the size of the test zone, which must be large enough to enclose the AUTs to be tested. Hence, as the electrical size of the AUT increases, the number of spherical modes required for the characterization of the AUT and test zone fields expands rapidly. This directly influences the size of the matrix and the computational requirements in the matrix inversion. In the general case, the size of the matrix, that is required to be inverted, is $2N(N+2) \times L$, where L is the number of measured probe signals. This matrix size sets the upper limit for the acceptable size of the AUT in wavelengths, for which the method is computationally applicable. For example, for $N = 40$ or greater, there are more than 10 million elements in the matrix, and the method can hardly be used. For such AUTs, the original TZF compensation method could still be used. The computational complexity of the modified TZF compensation is $O(N^6)$, whereas in the original TZF compensation it is $O(N^3)$ [22] [6].

In summary, a compensation method has been presented, which enables small-antenna pattern measurements in surroundings with an arbitrarily high reflectivity level, provided that the amplitude of multiple reflections is small compared to the primary reflections. The accuracy of the method is mainly determined by the uncertainties in the TZF measurement. Potential applications include measurements in normal, non-anechoic rooms and also multi-probe measurement systems, where the neighboring probes are an unavoidable source of reflections. The functioning of the method has been confirmed with measurement results.

ACKNOWLEDGMENT

M. Mustonen and J. Ilvonen are thanked for providing the antenna-model data for the simulations. S. Pivnenko is acknowledged for performing the measurements at the DTU-ESA Spherical Near-Field Antenna Test Facility and L. Nyberg and P. Rummukainen for helping with the measurements at Aalto University.

REFERENCES

[1] J. C. Bennett and A. Griziotis, “Removal of environmental effects from antenna radiation patterns by deconvolution processing,” in *Proc. IEE Conf.*, Pub. 219, Pt. 1, 1983, pp. 224-228.

[2] J. F. R. Pereira, A. P. Anderson, and J. C. Bennett, “New procedure for near-field measurements without anechoic requirements,” *IEE Proc. Microwaves, Optics and Antennas*, vol. 131, no. 6, pp. 351-358, 1983.

[3] J. Appel-Hansen, “Reflectivity level of radio anechoic chambers,” *IEEE Trans. Antennas and Propagation*, vol. 21, no. 4, pp. 490–498, Jul. 1973.

[4] J. van Norel and V. J. Vokurka, ”Novel APC-methods for accurate pattern determination,” in *Proc. Antenna Measurement Techniques Assoc. Symp.*, USA, 1993, pp. 385-389.

[5] W. D. Burnside and I. J. Gupta, “A method to reduce signal errors in antenna pattern measurements,” *IEEE Trans. Antennas and Propagation*, vol. 42, no. 3, pp. 399–405, Mar. 1994.

[6] D. N. Black and E. B. Joy, “Test zone field compensation,” *IEEE Trans. Antennas and Propagation*, vol. 43, no. 4, pp. 362–368, Apr. 1995.

[7] D. A. Leatherwood and E. B. Joy, “Plane wave, pattern subtraction, range compensation,” *IEEE Trans. Antennas and Propagation*, vol. 49, no. 12, pp. 1843–1851, Dec. 2001.

[8] S. A. Goodman and I. J. Gupta, “A method to correct measurement errors in far-field antenna ranges,” in *Proc. Antenna Measurement Techniques Assoc. Symp.*, USA, 2007, Paper A07-0068.

[9] A. C. Newell and G. Hindman, “Scattering reduction in spherical near-field measurements,” in *Proc. 2008 IEEE AP-S Int. Symp.*, San Diego, USA, Paper 439.3.

[10] D. W. Hess, “The IsoFilter technique: isolating an individual radiator from spherical near-field data measured in a contaminated environment,” in *Proc. 28th Antenna Measurement Techniques Assoc. Symp.*, Austin, Texas, USA, 2006, pp. 289–295.

[11] J. T. Toivanen, T. A. Laitinen, S. Pivnenko and L. Nyberg, “Calibration of multi-probe antenna measurement system using test zone field compensation,” in *Proc. 3rd Eur. Conf. Antennas and Propagation*, Berlin, Germany, 2009, pp. 2916-2920.

[12] J. E. Hansen, *Spherical Near-Field Antenna Measurements*. London, UK: Peter Peregrinus Ltd., 1988.

[13] F. Jensen and A. Frandsen, “On the number of modes in spherical wave expansions,” in *Proc. Antenna Measurement Techniques Assoc. Symp.*, Atlanta, Georgia, USA, 2004, Paper PID-105.

[14] T. Laitinen, “Spherical wave expansion –based measurement procedures for radiated fields,” Lic. Sc. thesis, Dept. Electrical and Communications Eng., Helsinki Univ. of Tech., Espoo, Finland, 2000.

[15] T. Kailath, A. H. Sayed, and B. Hassibi, *Linear Estimation*. New Jersey: Prentice Hall, 2000.

[16] M. Mustonen, “Multi-element antennas for future mobile terminals,” Lic. Sc. thesis, Dept. Radio Science and Eng., Helsinki Univ. of Tech., Espoo, Finland, 2008.

[17] DTU-ESA Spherical Near-Field Antenna Test Facility, specifications. Available: http://www.dtu.dk/centre/ems/English/research/facilities/facility_specifications.aspx

[18] T. A. Laitinen, J. Toivanen, C. Icheln, and P. Vainikainen, “Spherical measurement system for determination of complex radiation patterns of mobile terminals,“ *Electronics Letters*, vol. 40, no. 22, pp. 1392–1394, 2004.

[19] J. Toivanen, T. A. Laitinen, C. Icheln, and P. Vainikainen, “Spherical wideband measurement system for mobile terminal antennas,” in *Proc. 2nd IASTED Int. Conf. Antennas, Radar and Wave Propagation*, Banff, Canada, 2005, pp. 360-365.

[20] R. C. Wittmann, “Spherical near-field scanning: determining the incident field near a rotatable probe,” in *1990 Antennas and Propagation Symp. Dig.*, 1990, pp. 224-227.

[21] F. Jensen, “On the probe compensation for near-field measurements on a sphere,” *Archiv fuer Elektronik und Uebertragungstechnik*, vol. 29, pp. 305–308, Jul. 1975.

[22] F. Holm Larsen, “Probe-corrected spherical near-field antenna measurements,” Lic. Sc. thesis, Electromagn. Inst., Tech. Univ. of Denmark, Lyngby, Denmark, 1980.